SEASONAL CHARACTERISTICS OF PRECIPITATING CLOUD PROPERTIES AND STRUCTURES IN THE INLAND OF THE INDOCHINA PENINSULA: A LEGACY OF 16 YEARS OF THE TROPICAL RAINFALL MEASURING MISSION (TRMM) SATELLITE

***Nattapon MAHAVIK*[1*], *Sarintip TANTANEE*[2]**

DOI: 10.21163/GT_2021.161.05

ABSTRACT:
Seasonal characteristics of cloud properties and structure based on mesoscale properties of precipitation systems over the inland Indochina Peninsula (IP) and surrounding regions during the years 1998-2013 were investigated in this study. Using daily product from Tropical Rainfall Measuring Mission, the monsoon season, firstly, was demarcated to find onset and withdrawal dates for each year, and then to divide the period into the premonsoon, monsoon and postmonsoon seasons. In the 16-yr "climatology", on average, the variations were found both in physical properties and structures of precipitation features (PFs) for each season. Based on applied definition, the intra-seasonal and the inter-seasonal variation of rainfall intensity and periodical duration length were considered to identify the seasonal period of each year. Mesoscale Convective Systems (MCSs) played a significant role through their contribution of rainfall for all periods. Sub-MCSs were major contributors of rainfall during the postmonsoon season, while the highest percentage of intense MCSs (IMCSs) was found in the premonsoon season. The enhancement of IMCs for the premonsoon season is the largest over the inland IP based on microwave signal and radar reflectivity sensors. Distinct spatial concentration was found over west and north IP for sub-MCSs during monsoon seasons. Convection intensity proxies and vertical radar reflectivity demonstrate intra-seasonal variation over land, were identified through cumulative density function analysis by enhancement of MCSs during the premonsoon season. Spatial distribution of PFs based on maximum height cloud average over the inland IP has shown at height exceeding 8 km over the western inland IP during premonsoon season. Spatial variation of the microphysical structure of cloud is distinctly shown by seasons based on scattering of microwave signals, and lightning flash counts. The most frequent lightning was found during premonsoon season over inland IP, while the most flash count average was also found over inland IP especially over west, north in highland of IP during premonsoon season. Further study should be conducted to analyze on seasonal periods for understanding on the variations of microphysical structure and cloud properties.

Key-words: *TRMM 16 years, Cloud Structure, Indochina Peninsula, Convective Cloud, Precipitation Features*

1. INTRODUCTION

Rainfall characteristics and dynamic-thermodynamic environments vary from regions to regions. Characteristics of convective cloud differ by areas based on topography and atmospheric forcing. For instance, Xu (2013) found that mixed phase process on precipitation play more significant role over the south of China more other regions. Some extreme convective hot spots, observed by three-dimensional precipitation radar retrieved from Tropical Rainfall Measuring Mission (TRMM), are founded on the steep slope and foothill regions in South America. Meanwhile, some intense convective features are located over the southwest foothills of the Himalayas (Zipser et al., 2006; Houze et al., 2007; Medina et al., 2010; Romatschke & Houze, 2010). Understanding these spatial and temporal variations in rainfall characteristics using satellite observation is crucial for building knowledge for disaster prevention in Indochina Peninsula (IP). The IP is the region located within the

[1]*Department of Natural Resources and Environment, Faculty of Agriculture Natural Resources and Environment, Naresuan University, Phitsanulok, 65000, Thailand, nattaponm@nu.ac.th*
[2]*Centre of Excellence on Energy Technology and Environment, Faculty of Engineering, Naresuan University, Phitsanulok, 65000, Thailand, sarintipt@nu.ac.th*

region of the Asian monsoon. The IP is defined as a transitional zone between two Asian monsoon systems (Wang and Ho 2002). TRMM was launched in 1997 and ceased data collection in April, 2015 (Li et al., 2019). The TRMM project was the first space-borne radar observation precipitation radar (PR) with additional sensors, including TRMM Microwave Imager (TMI), the Visible and Infrared Radiometer System (VIRS), the Clouds and Earth's Radiant Energy System (CERES) and the Lightning Imaging System (LIS) (Kummerow et al., 1998). Long-term accumulated data based on TRMM observations can be used to describe the climate features of rainfall and its properties. Vertical profiles and horizontal variations in radar reflectivity have been used to investigate the climatic features at different times (e.g. Petersen & Rutledge, 2001; Petersen et al., 2002; Kodama et al., 2005; Xu et al., 2009).

Understanding microphysical precipitation characteristics over the tropics is one of the keys to elucidating climate change (Kodama et al., 2015; Satoh et al., 2018). The two types of precipitating clouds in the tropics are convective and large stratiform rain areas, which are, in the main part, embedded in mature mesoscale convective systems (MCSs) (Houze, 1989). Both convective precipitation and stratiform precipitation coupled within Tropical Cyclones, resulting a long duration of rainfall can cause the damage and deaths from flooding (Jorgensen, 1984; Yokoyama & Takayabu, 2008). Therefore, it is necessary to understand MCSs embedded in Precipitation Features (PFs) over the tropics. Nesbitt et al. (2000) developed an algorithm to identify PFs using data from TRMM PR and TMI. Based on definition MCSs from (Houze, 1993), precipitation systems can be successfully described from the convective intensity and rainfall distributions over the tropics. The finding has clearly shown that such features which develop over land are much more intense than similar oceanic features. Although the TRMM mission ended in 2015, related studies are still ongoing based on the PR data in storage. The University of Utah Precipitation Measuring Missions (PMM) science group has produced its work using all primary data retrieved from TRMM sensors on PF studies (Nesbitt et al., 2000; Liu et al. 2008; Liu, 2013). The event-based reanalysis database of PFs has collocated TRMM data to generalize precipitation and cloud features as well as study the radar, passive microwave and lightning characteristics of precipitating systems in the tropics. Many studies have been carried out using this database, including rainfall estimates validation, diurnal cycle of precipitation systems, global distribution of storms with LIS-detected lightning, deep convection reaching the tropical tropopause layer rainfall production and convective organization, and the categorization of extreme thunderstorms by their intensity proxies (Nesbitt et al., 2003; Nesbitt et al., 2004; Cecil et al., 2005; Liu & Zipser, 2005; Zipser et al. 2006).

In addition, there have been many studies to describe regional variation on PFs over the tropics using TRMM data. In Asia, for example, studies of the organized convective systems characteristics in eastern Asia, such as Mei-yu seasons, used the TRMM PF database (Xu et al., 2009). Besides, Guy & Rutledge (2012) investigated climatology of MCSs associated with the West African monsoon using TRMM PR and TMI based on 13-year (1998–2010) from the University of Utah TRMM PF database. Convective intensity metrics indicate that land-based systems exhibit stronger characteristics, such as higher storm tops, maximum 30 dBZ heights, and significant 85 GHz brightness temperature depressions. Rapp et al. (2014) investigated the role of storm characteristics on the seasonal and diurnal cycles of precipitation in four distinct regions of Costa Rica by utilizing The University of Utah TRMM PF database. They found that the relative importance of convective precipitation increases on the Caribbean side during wintertime cold air surges. However, there are still gaps on studying of spatial and temporal variability in the convective cloud properties and structure in the Inland IP using the TRMM PF database.

In this study, our aim is to focus on precipitation structure and its properties using a TRMM dataset over the inland of IP and surrounding area. Most of the figures were produced using the Python script. This paper comprises of four sections. Section 1 provides some background and an introduction. Section 2 describes data and methodology: study area, the datasets, and definition of monsoon periods, the PFs database, and interpretation of PF parameters. Section 3 describes the results and discussion: finding monsoon season periods, Classified PFs, and spatial distribution on PFs properties. The conclusion is given in section 4.

2. DATA AND METHODOLOGY

2.1 Study Area

The Indochina Peninsula (IP) and surrounding areas demonstrate spatial variation of annual precipitation (**Fig. 1a**). Less annual rainfall occurs in the middle part of the IP, while large amounts fall over the coastal regions and surrounding seas. Moisture transportation from the Indian and Pacific Oceans contributes to annual rainfall in the IP during monsoon seasons. The rainfall variability over the IP is mainly influenced by the southwesterly monsoon from the Indian ocean during the first half of the summer monsoon and from the Pacific Ocean during the latter half (e.g., Matsumoto 1997, Takahashi &Yasunari 2006). In addition, topography is also a key factor in controlling the amount of rainfall over the IP (**Fig. 1b**). A mountainous region is located across the northern IP, while narrow and steep mountain ranges and basins are found in the middle part of the IP (**Fig. 1b**).

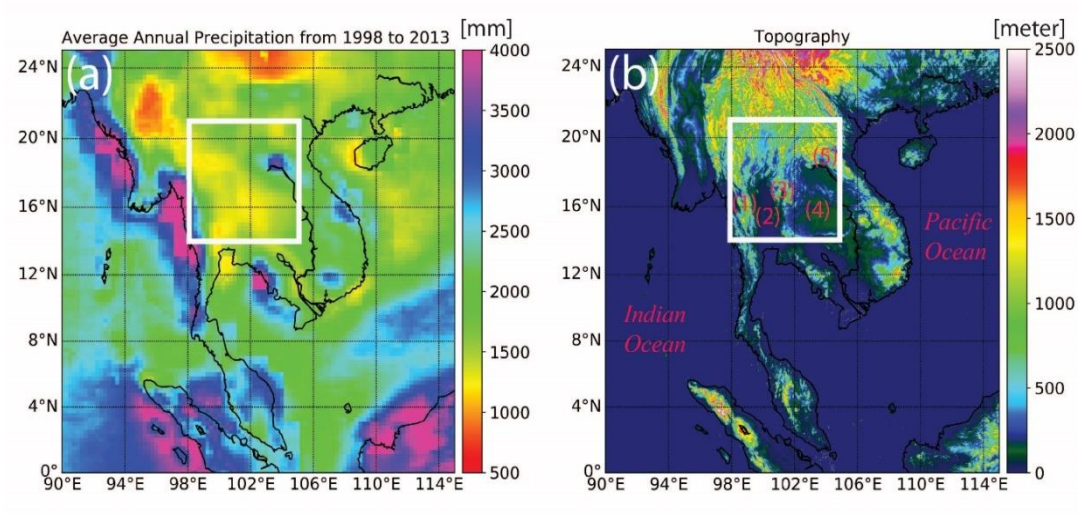

Fig. 1. Study area (a) annual precipitation average from 1998 to 2013 from TRMM3B42. White solid box represents study area for analysis of convective cloud properties and structures (b) Topography of the study area and surrounding area over Indochina. Locations referred in text include 1) Tenasserim mountain range, 2) Chao Phra Ya basin, 3) Phetchabun range, 4) Khorat basin, 5) Annamite mountain Range.

2.2 TRMM Dataset

2.2.1 TRMM Version-7 3B42 Dataset

The primary sources of data are from sensors on board the TRMM satellite namely PR, TMI, and LIS (Kummerow et al., 1998). The TRMM PF database (Nesbitt et al., 2000; Liu et al., 2008) from link http://atmos.tamucc.edu/trmm/data/trmm/level_2/rpf/ is used to assess rainfall characteristics and convective cloud properties over inland IP from 1998 to 2013. In addition, to define seasons, the TRMM version-7 3B42 from link https://disc.gsfc.nasa.gov/mirador-guide is employed (Huffman et al., 2007). TRMM3B42daily Version 7 has spatial resolution of 0.25° x 0.25° located from 50° S to 50° N with the collecting period from 1998 to 2014, and it continues as an ongoing global precipitation measurement (GPM) project. The infrared radiance measurements from geostationary satellites provide the primary source of rain estimates, which are calibrated by passive microwave sensors, including TMI and PR, on board TRMM.

2.2.2 TRMM Precipitation Feature Database

A new version of the PF database that was reprocessed in 2012 based on TRMM product version 7 (Liu, 2013) is used to analyze convective characteristics inland IP for a 16-year period (1998-2013) before starting GPM. The PF database was developed by Liu et al. (2008), based on Nesbitt et al. (2000) algorithm. The PF database was updated to new version in 2008 by including both PFs and cold cloud features (Liu et al., 2007) to account for warm rainfall under clouds without ice. The PR-detected Precipitation Feature (RPF) is used due to the combination level-2 files from monthly statistics are easily built. The PF database incorporates many standard product outputs (e.g., 2A25; TRMM PR3-D reflectivity) along with calculated statistics (e.g., min 85 GHz microwave brightness temperature) (Liu et al., 2008). The PF algorithm is used to define PFs by grouping contiguous rain area originally observed by the TRMM Precipitation Radar (PR) and Microwave Imager (TMI). Therefore, the properties of each PF, such as size, rain volume, and convective intensity proxies (e.g., lightning flash rate, height of radar echoes) can be summarized.

2.3 Methodology

As shown in **Fig. 2**, the TRMM data set was used in the analysis. Firstly, the periods of monsoon seasons were defined and calculated based on TRMM 3B42. Then, the analysis of PFs was done using TRMM PF database to understand precipitation structure and its. Properties based on defined monsoon periods.

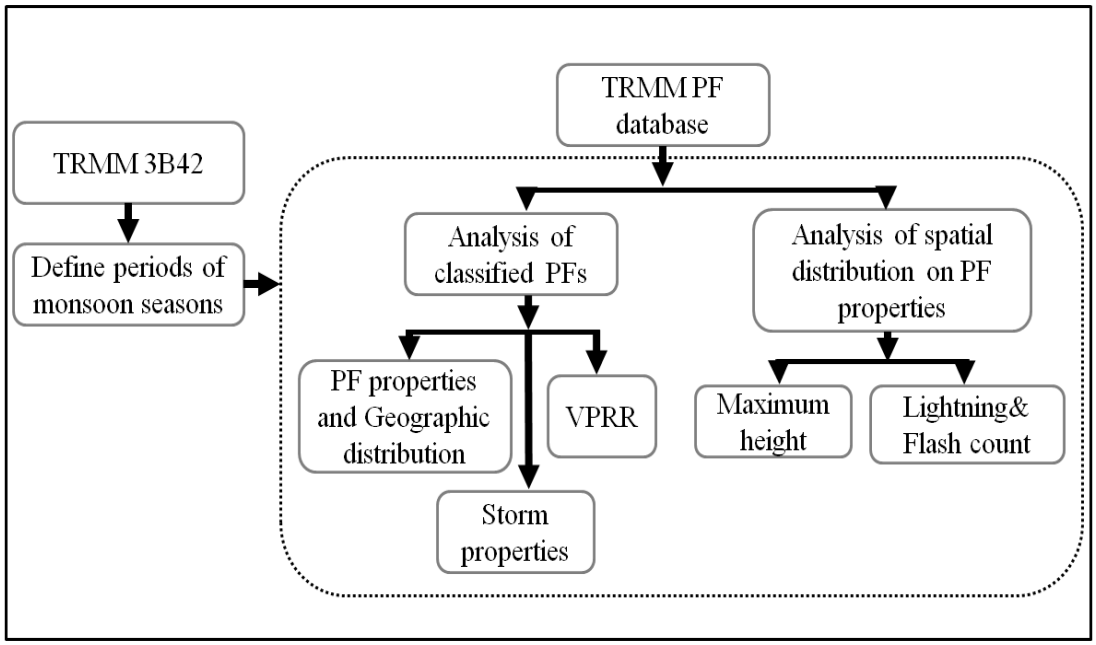

Fig. 2. Flowchart of the study.

2.3.1 Definition of Monsoon periods

To define the periods of monsoon seasons, onset and withdrawal dates, using 5-day mean (pentad), must be defined based on Matsumoto (1997). Specifically, the 5-day mean rainfall computed from daily rainfall TRMM3B42 is considered with annual mean pentad (Pm = (Annual precipitation)/73). Matsumoto (1997) defined onset and withdrawal pentad for each rain gauge

station, while this study, with its specific interest in the inland IP, defines the whole study area (**Fig. 1**). Therefore, the onset and withdrawal pentads are representative for the white box (**Fig. 1a**).

The definition of the onset (withdrawal) of summer rainy season is that the first (last) pentad in which the mean pentad precipitation exceeds Pm in at least three consecutive pentads after (before), dropping it in more than three consecutive pentads. The onset and withdrawal dates are defined as the middle date of the defined pentad. Therefore, the monsoon period for each year can be defined from the onset date to one day prior to the withdrawal date. The premonsoon period can be defined from 1st February to one day prior to the onset date. Finally, the postmonsoon period is defined from withdrawal date to 30th November.

2.3.2 Classification of PF

The PFs are analyzed for two regions based on analysis purposes. The first region (14° -21° N, 98° -105° E) is defined for analysis of convective cloud properties and structures over the inland IP, while the second region (0° -25° N, 90° -115° E) is a subset area used for discussion of spatial distribution of PFs. In this study, the PFs are analyzed in three periods of premonsoon, monsoon and postmonsoon. Areas and the presence of convective pixels are used as condition to classify further the selected PFs into MCSs, intense MCSs, sub-MCSs, or non-convective systems (NCs) (Xu et al., 2009). The area used to define MCSs is based on the definition by Houze (1993) used in Xu et al. (2009). PFs with an area greater than 1000 km^2 containing at least one convective pixel are classified in MCSs. Intense MCSs are classified separately from MCSs when the maximum height of 30 dBZ echo is higher than 8 km. Sub-MCSs are defined as PFs with an area less than 1000 km^2 and occupying at least one convective pixel. Finally, NCs are the systems without any convective pixel, indicating decayed convective systems or stratiform systems.

2.3.3 PF Interpretation Parameters

Radar Reflectivity: Many parameters of PFs derived from PR, TMI and LIS are used in analysis of convective cloud properties and structures. PR parameters used are area coverage of PFs, maximum radar reflectivity, maximum height of 30-dBZ echo, and maximum radar echo at the height of 6 km. The supercooled liquid droplets or large ice particles is presented by high values of radar reflectivity above the freezing level. The maximum height of 30-dBZ echo indicates the updraft level which supercooled liquid raindrops or large ice particles can be lifted (DeMott & Rutledge, 1998). Echo height of 6 km can refer to electrical phenomena when echo exceeds the value of 35-40 dBZ in the mixed-phase region (where $0^\circ C \geq T \geq -40^\circ C$) with temperature lower than -5° C reported by many studies (Dye et al., 1989; Williams et al., 1992; Petersen et al., 1996; Petersen et al., 1999). The convective cores are presented by Vertical profiles of radar reflectivity (VPRR) retrieving from maximum reflectivity factors of precipitation systems as a function of height (Donaldson, 1961; Zipser & Lutz, 1994; Xu et al., 2009).

*Passive Microwave Brightness Temperature:*To prevent mix-up with low brightness temperatures caused by low surface emissivity of ice scattering, Polarization Corrected Temperature at 85 GHz from TMI (85-GHz PCT) is derived from conversion of polarization for both horizontal and vertical signals (Spencer et al. 1989). The 85-GHz PCT responds to upwelling scattered background radiation caused by ice particles lifted by the updraft as a proxy for ice water content integrated over depth (IWP) (Vivekanandan et al., 1991). The lower GHz PCT, the more enhanced IWP responds to strong convective intensity (Mohr & Zipser, 1996; Cecil & Zipser, 1999; Zipser et al., 2006).

Interpretation of PF Parameters Measured from LIS: A strong updraft can produce supercooled cloud liquid water and large heavily rimed graupel particles in the mixed-phase clouds (Williams, 1989). The collision between small size of ice particles with large size of graupel, producing the supercooled liquid water can induce charge separation leading to lightning (Saunders, 1998).

3. RESULTS AND DISCUSSION

In this section, the classification on monsoon seasons from 16 years of TRMM data is described on the results. The concept of rainfall in pentad (5 days) is used to compute in finding the onset and withdrawal dates on summer monsoon season of each year.

3.1. Finding Monsoon Season Periods

Based on method of defining monsoon from Matsumoto (1997), the daily rainfall estimates from 16 years of TRMM data had been done over the white boundary box of the central area of the IP (**Fig. 1a**). The onset and the withdrawal of monsoon pentads had been calculated for each year. The period of premonsoon, monsoon, postmonsoon dates were found for each year, depending on annual variation of rainfall amount. The premonsoon starting date is defined as the 1st of February annually, while last date of the postmonsoon is defined as being the end of November annually. The monsoon onset and withdrawal dates provide information about the wet and dry years. A longer duration of the monsoon season means more rainfall above the annual pentad mean for each pentad. In this study, dry spell periods are not considered during monsoon periods due to few and noncontiguous pentads.

Using 2011 as an example, annual rainfall is relatively larger than average annual rainfall (**Fig. 1b**) over the inland IP (**Fig. 3a**). To find seasonal periods of each year, the pentad mean rainfall is computed over the white solid box (**Fig. 3a**). In **Fig. 3b**, Pentad Numbers 21 and 58 are defined as onset and withdrawal pentads for 2011.

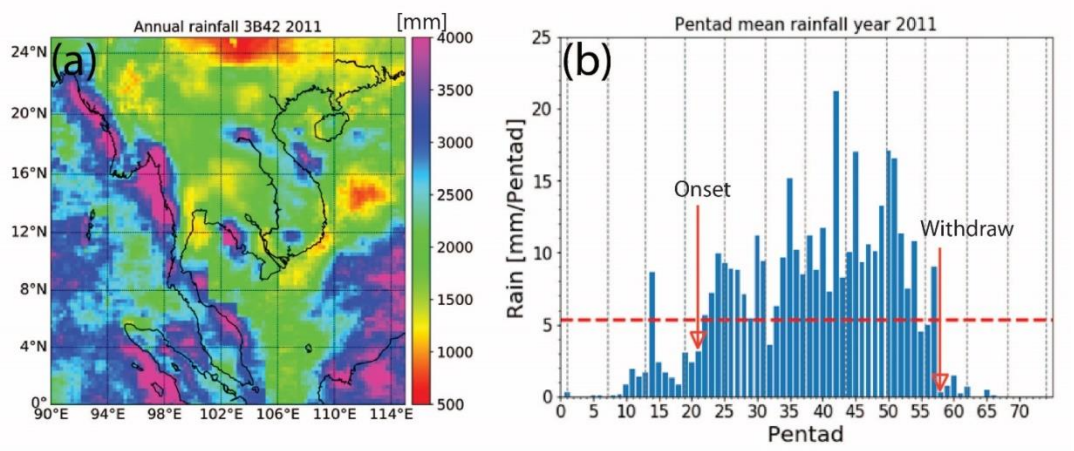

Fig. 3. Seasonal periods defined: (a) annual rainfall in 2011 (b) pentad mean rainfall in 2011. Red-dashed horizontal line indicates annual mean pentad.

Inter-annual variations of rainfall periods are shown in **Table 1**. For example, the early onsets in 1999 and 2006 started on pentad number 19, while the longer monsoon period occurred in 1999. Variation of mean rainfall was also observed. In 2011, the highest mean rainfall caused massive flooding in the Chao Phraya basin, where locates in the middle of the IP.

3.2. Classified PFs

In this section, precipitation feature and geographical distribution is investigated on classified monsoon seasons and analyzed with classified PFs based on criteria mentioned in section 2.2.3. Next, the storm properties over the inland IP were analyzed using mentioned criteria in section 2.2.3. The vertical profile of radar reflectivity (VPRR) for classified seasons is also investigated and compared among classified PFs.

Table 1.
Sixteen years of statistics for seasons defined by TRMM observations from 1998 to 2013.

Year	mean rain (mm)	Onset PT	Withdrawal PT	Num Pre-MS Dates	Num MS Dates	Num Pt-MS Dates
1998	3.7	25	58	97	166	44
1999	4.9	19	61	67	211	29
2000	4.9	21	56	77	176	55
2001	4.7	23	60	87	186	34
2002	5.0	23	61	87	191	29
2003	4.1	24	58	92	171	44
2004	4.3	22	53	82	156	70
2005	4.5	24	56	92	161	54
2006	4.8	19	57	67	191	49
2007	4.4	23	57	87	171	49
2008	5.0	21	56	77	176	55
2009	4.2	24	59	92	176	39
2010	4.4	26	59	102	166	39
2011	5.3	21	58	77	186	44
2012	4.5	22	56	82	171	55
2013	4.7	23	59	87	181	39

3.2.1 PF Population and Geographical Distribution

MCSs made a significant contribution to rainfall over the inland IP in all periods. Based on the white solid box **(Fig. 1a)** the total sample of 21,171 PFs were found over the inland IP during three periods (**Table 2**). About 24% fall into NCs class, while a large number of PFs, about 72% fall in Sub-MCSs class. Only 2.3% of the PFs reach the threshold of MCSs, with only 1.7% of these reaching the threshold definition of intense MCSs. The sample size of monsoon PFs is the largest, followed by the premonsoon and the postmonsoon seasons, respectively, due to the defined periods based on Matsumoto (1997). The premonsoon season has the largest percentage of intense MCSs and NCs compared to other periods. On the other hand, the small convective systems of Sub-MCSs comprise the largest percentage of the classified PFs during the postmonsoon season.

Table 2.

Precipitation Features.

Period/type	Tot PFs No.	NCs		Sub-MCSs		MCSs		Intense MCSs	
		No.	%	No.	%	No.	%	No.	%
Pre-MS		2296	30.6	4838	64.5	154	2.1	205	2.7
Monsoon		17884	26.5	46356	68.8	1954	2.9	1079	1.6
Post-MS		991	13.9	5951	83.4	128	1.8	59	0.8
Tot		21171	23.7	57145	72.2	2236	2.3	1343	1.7

Geographically, MCSs concentrate in the western part of the inland IP, over the Tenasserim mountain range, during monsoon (**Fig. 4b**), while they are found with greater frequency over the southern part of the IP and near the equator for both land and ocean in premonsoon and postmonsoon seasons (**Fig. 4a** and **4d**), respectively. Sub-MCSs is located in the western and northern regions of the inland IP during monsoon (**Fig. 4e**) and they occur with greater frequency over ocean areas during premonsoon and postmonsoon seasons (**Fig. 4d** and **4f**).

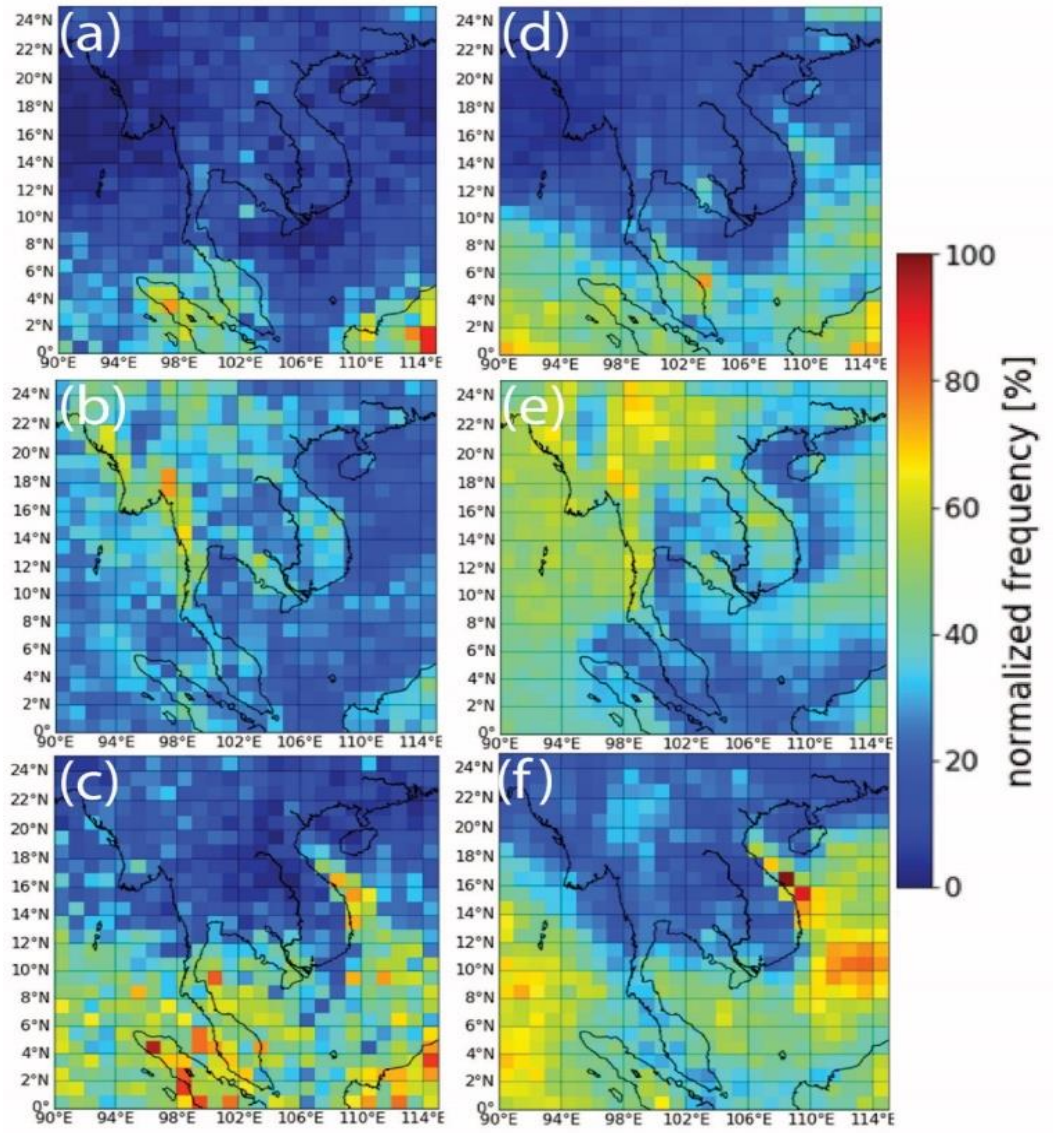

Fig. 4. Frequency occurrence of classified PFs for premonsoon, monsoon, and postmonsoon (a), (b), (c) for MCSs (d), (e), (f) for sub-MCSs.

3.2.2 Storm Properties over the Inland IP

Median values and their cumulative distribution functions (CDFs) are shown in **Table 3** and **Fig. 5**, respectively. The area is calculated from parameters named "NPIXELS_PR" that is the number of pixels observed by PR. The altitude of spacecraft's orbit before and after booting are considered due to the direct effect to horizontal resolution.

Table 3.

Median values of selected parameters.

Period	Type	Area	Min85pct	Maxht30	Maxdbz6
Pre-MS	Tot PFs	26.0	276.6	5.0	22.5
	MCSs	617.4	244.0	6.0	33.3
	IMCSs	1300.5	168.3	11.3	48.0
Monsoon	Tot PFs	26.0	277.7	4.8	22.0
	MCSs	494.2	238.1	6.0	33.6
	IMCSs	1248.5	164.4	10.0	45.0
Post-MS	Tot PFs	26.0	279.6	4.3	21.6
	MCSs	598.2	248.3	5.6	31.7
	IMCSs	1196.5	173.0	10.0	43.2

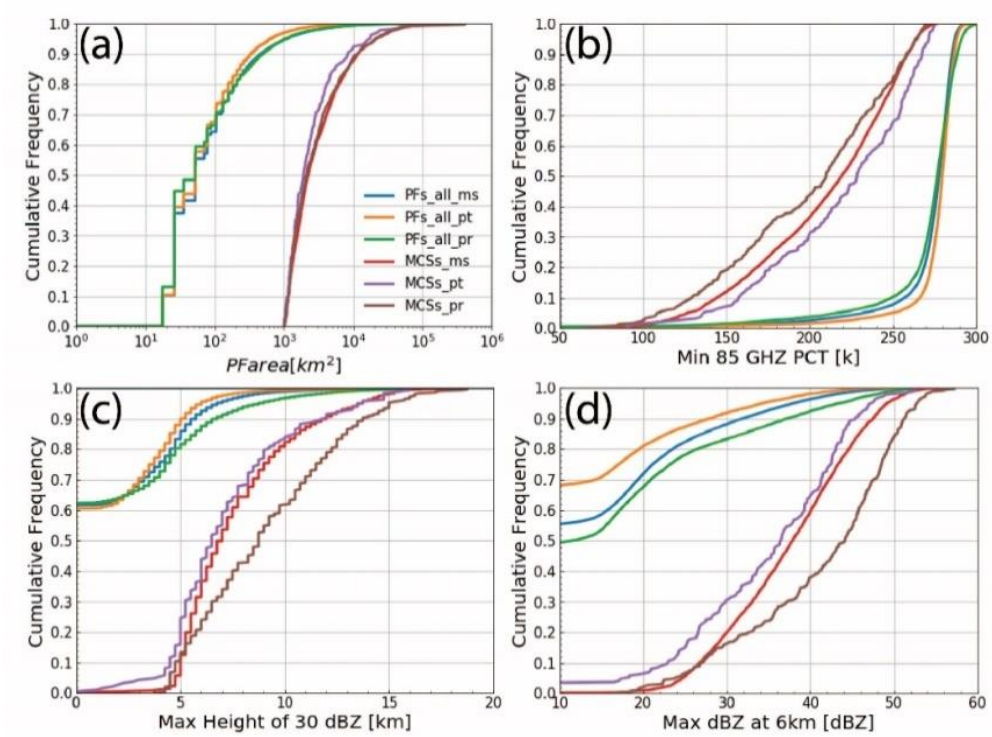

Fig. 5. Cumulative Density Function of statistics extraction from premonsoon, monsoon, and postmonsoon (a) area, (b) min PCT of 85 GHz, (c) max height of 30 dBZ, and (d) max dBZ at 6 km, for all PFs and MCSs over inland Indochina from solid white box, as shown in **Fig. 1a**.

1) Area Structure

PFs of different seasons do not differ in area size when all the PFs are analyzed (**Table 3** and **Fig 5a**). The PFs in small features dominate more than 95% being at area size smaller than 1000 km^2. However, only the more intense systems are considered, differences in area structures are found of PFs by seasons. The largest-area MCSs are found in the premonsoon season, but the frequency of

IMCSs is not very different between premonsoon and monsoon seasons. Relatively smaller IMCSs are found in the postmonsoon season.

2) Statistics for convection intensity proxies

As shown in **Table 3**, median values for IMCSs during postmonsoon are the most severe compared to other periods, except for Min85PCT for monsoon season. Taller and stronger clouds (MaxHT30; MaxdBZ6) derived from PR on board TRMM are enhanced over the inland IP in the case of IMCSs. PFs with very weak intensity dominate in the study area presenting by high PCT values according to CDFs of minimum 85-GHz PCT (Min85pct; **Fig. 5b**). Only about 10% of the total features have values less than 250 K, which is used as the threshold to delineate systems with low rain intensity (Spencer et al., 1989). Only about 5% of all PFs indicate for the deep convection using threshold lower than 225 K following McGaughey et al. (1996).

More than 60% of all PFs does not have sufficiently large hydrometeors concentration to produce a 30-dBZ radar echo (**Fig. 5c**). Besides, the shallow PFs less than 6 km are found about 50% (**Fig. 5d**). In contrast to shallow PFs, more than 90% of MCSs are found to exceed a height of 6 km. A small fraction of MCSs is found with radar echoes at 30 dBZ reaching up to 15 km, and 6 km radar echo exceeding 50 dBZ. The strong MCS intensity during premonsoon is observed through ice scattering signal (Min85pct), vertical radar reflectivity (MaxHT30; **Fig. 5c**), and maximum radar reflectivity at 6 km (MaxDbz6; **Fig. 5d**). The MCS intensity is ordered from stronger to weaker by premonsoon, monsoon and postmonsoon, respectively. About 40% and 60% of features for both maximum height at 30dBZ (**Fig. 5c**) and Max dBZ at 6 km (**Fig. 5d**), which exceed for both height of 10 km and 40 dBZ, are found in premonsoon period. The statistics indicate the presence of larger super-cooled raindrops in the mixed-phase clouds during premonsoon season that are larger than those found in Xu et al. (2009). In addition, Guy & Rutledge (2012) used the same database PFs for 13 years that are shorter period than this study to assess convective characteristics from May to October during period of African Easterly Waves. They found that mean vertical profiles of convective were stronger in the location of continental interior. However, this study shows that MCSs of the premonsoon period over the inland is stronger and higher than other seasons that are different from Guy & Rutledge (2012) found during monsoon period.

3.2.3 Vertical Profile of Radar Reflectivity

The reflectivity profiles as a function of height are based on VPRR from Donaldson (1961), which is used to produce the PF product MaxdBZ (Xu et al. 2009). VPRR is produced from radar echoes observed by TRMM PR at a vertical resolution of 0.25 km, from the TRMM precipitation and cloud feature database (Liu, 2013). VPRR indicates storm intensity respected to radar echo above the mixed-phase region (Szoke & Zipser, 1986; Zipser & Lutz, 1994; Cecil et al., 2005; Xu et al., 2009). However, recent study shows that the extreme rainfall events are mostly associated with less intense convection (Hamada et al., 2015).

Fig. 6 shows the VPRR for MCSs and Sub-MCSs in the inland IP during the defined periods. MCSs with more intense convection according their extending echo top height are found compared to those of sub-MCSs. The maximum radar height for MCSs reaches to a height of more than 18 km for the premonsoon season. The MCSs intensity during premonsoon is the strongest among the three seasons (**Fig. 6a**), while monsoon and postmonsoon periods are in close proximity (**Fig. 6b** and **6c**), indicating no significant difference in the convective structures. Sub-MCSs for both premonsoon and postmonsoon indicate stronger intensity than during the monsoon season, with height exceeding 15 km (**Fig. 6d**, **6e**, and **6f**).

In this study, stronger radar echoes between 2 and 5 km for MCSs are observed during premonsoon than during other periods. This enhanced radar reflectivity may be generated from the mixed-phase region of the premonsoon season. Compared to sub-MCSs over the South China from Xu et al. (2009), the inland IP has a wider range of radar echoes and heights for all periods. Larger liquid drops or precipitation-sized ice particles can be found in the mixed-phase region where a higher potential for charge separation exists (Dye et al., 1989).

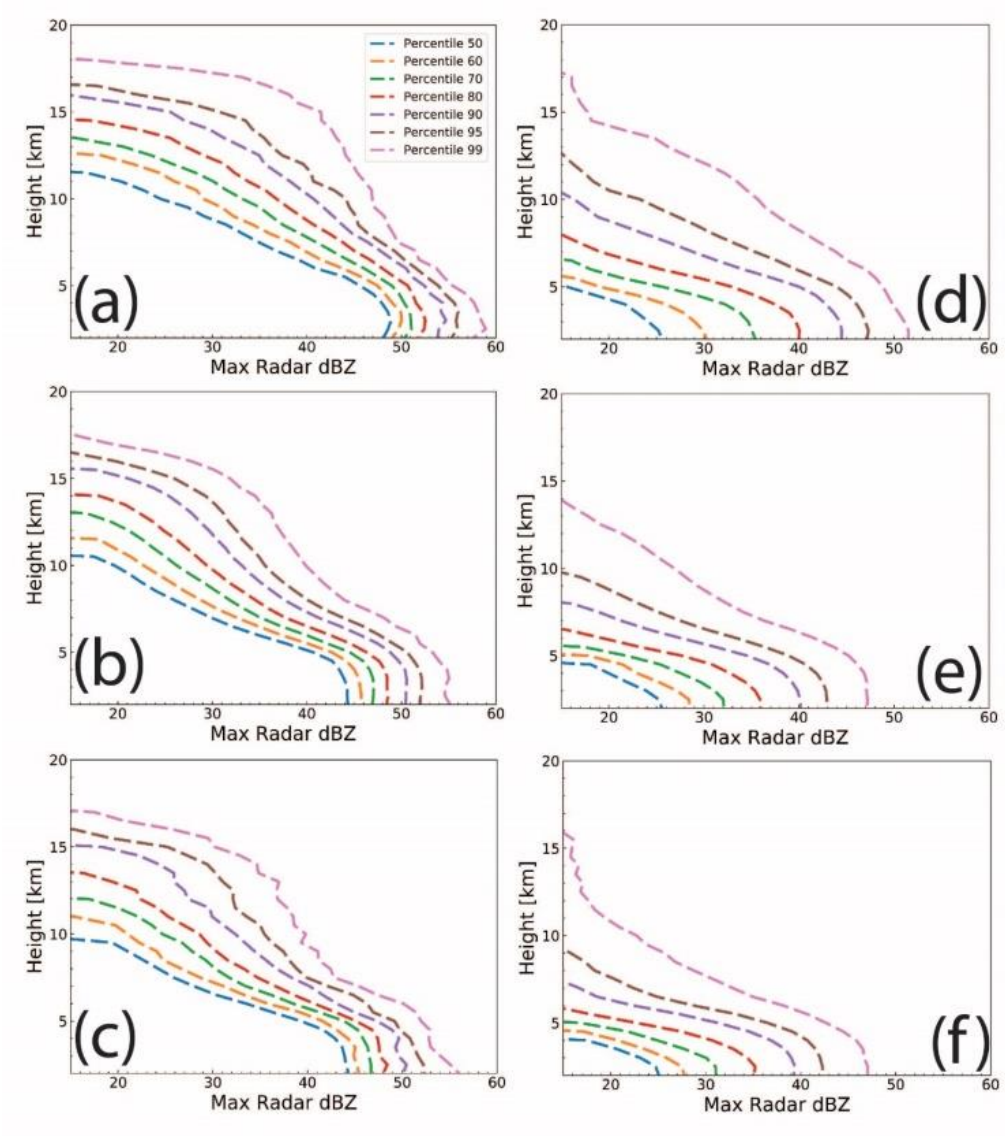

Fig. 6. Vertical profiles of radar reflectivity (from bottom to top in 50th, 60th, 70th, 80th, 90th, 95th, and 99th percentile) over inland IP during premonsoon, monsoon, and postmonsoon: (a),(b),(c) for MCSs; (d),(e), (f) for sub-MCSs. Data used for statistical calculations are from those grids inside the solid white box, as shown in **Fig. 1a**.

Table 4.

Precipitation Features with flashes counted over inland Indochina.

Period/criteria	PFs with flashes		With 1-9 No.	With 10-99 No.	With >=100 No.
	No.	%			
Pre-MS	566	7.5	412	136	18
Monsoon	2093	3.1	1749	338	6
Post-MS	116	1.6	103	13	0

As identified by Xu et al. (2009), lightning activity is one of the proxies used to examine convective activity. The lightning activity before monsoon onset is higher than other periods (Petersen et al., 2002; Xu et al., 2009; Williams et al., 1992; Qie et al., 2003; Yuan & Qie, 2008). In this sub section, the flash rate is analyzed for all three seasons. Not surprisingly, the highest flash rate of 7.5% was recorded during premonsoon over inland IP (**Table 4**). The flash rate decreases only 4 times from class 10-99 to class 1-9 in case of premonsoon seasons, while the monsoon abruptly decreases 5 times. The highest flash rate (>=100) was not observed in the postmonsoon season. In this study, the flash rate found in the inland IP is similar to that observed over the South China by Xu et al. (2009) during the premonsoon season.

Table 5.

Total flash counts.

Period	PFs	NCs	Sub-MCSs	MCSs	IMCSs	Rain area	Conv area
	Flash No.	Flash No.	Flash No.	Flash No.	Flash No.	(km^2 / flash)	(km^2 / flash)
Pre-MS	7638	10	1227	216	6118	205.5	77.8
Monsoon	13669	28	2268	414	10841	653.6	181.9
Post-MS	691	0	107	23	560	366.1	163.0

As shown in **Table 5**, flash rate caused by intense MCSs is larger than 80% in all seasons. Sub-MCSs are the second-ranked contributors for flash rate, followed by MCSs. The smallest rain area per flash occurs in the premonsoon season, followed by postmonsoon and monsoon seasons, which is consistent with the flash rate normalized by the convective area. When compared with pre-meiyu season, the normalized flash count over the inland IP in the premonsoon season is about three times less than that observed over southern China (Xu et al., 2009). This may be due to the fact that their study area including PFs over sea, which produce less lightning (Nesbitt et al., 2000).

3.3. Spatial Distribution on PF Properties

In this section, the spatial distribution of PF properties is analyzed on maximum height of PFs. In addition, the spatial distribution of Lightning and Flash Count is also investigated and disussed on the classified seasons with the classified PFs.

3.3.1 Maximum Height of PFs

Maximum height of PFs (MaxHT) can be used as one of the cloud characteristic proxies to investigate severity of precipitating cloud. Spatial variation in both frequency of occurrence and MaxHT average is clearly shown on the seasonal variation pattern (**Fig. 7**). A relatively low frequency of MaxHT is found during the premonsoon season over the inland IP compared to near equatorial regions (**Fig. 7a**), while the average height of PFs is relatively taller than that found during other periods over the inland IP, with approximate height exceeding 8 km (**Fig. 7d**). The highest frequency MaxHT was found inland of the northern ICP during monsoon (**Fig. 7b**). The frequency of the highest MaxHT over southern SCS, Bay of Bengal and Andaman Sea increases during postmonsoon season (**Fig. 7c**). The tallest average MaxHT were observed in the premonsoon season over the inland IP, compared to PFs over sea and other seasons (**Fig. 7d**). The tallest PFs are located over the middle part of Myanmar. The spatial pattern of average MaxHT shows a similarity of distribution between monsoon and postmonsoon seasons (**Fig. 7e** and **7f**). There were clearly spatial variations of MCSs and Sub-MCSs in the inland IP during premonsoon. In Western and central Africa, Balogun et al. (2020) analyzed TRMM PF database and detected echoes at high altitude much more frequently in the rainforest and savannah zones during March‐May, but the savannahs, Sudano, and Sahel zone convections tend to reach higher altitude more frequently than the rainforest zones during June‐September.

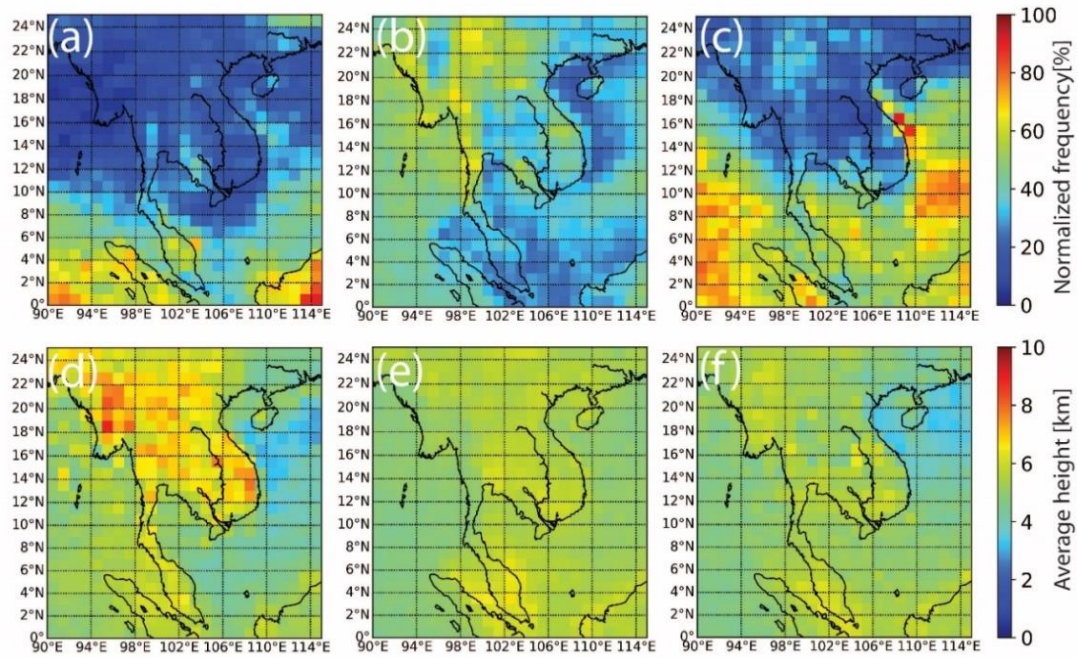

Fig. 7. Spatial distribution of MaxHT over IP and vicinity during premonsoon, monsoon, and postmonsoon. (a), (b), (c) represent frequency occurrences; (d), (e), (f) represent averages. The resolution grid size is at 1° degree.

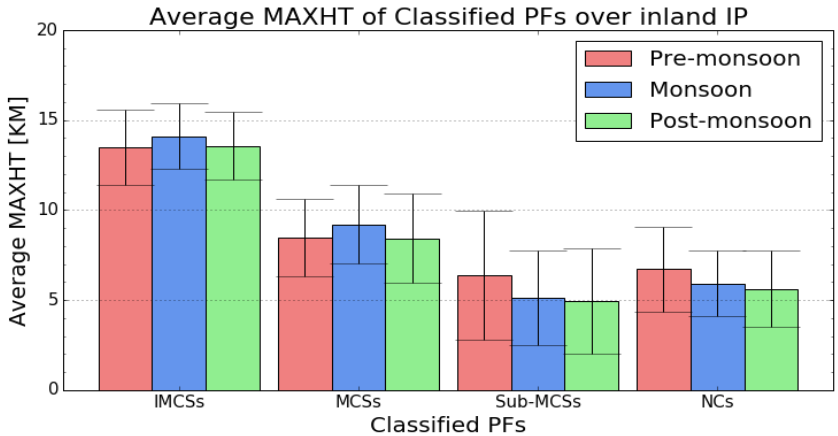

Fig. 8. Average MaxHT and standard deviation of classified PFs over solid white box shown in **Fig. 1a** during premonsoon, monsoon, and postmonsoon. Data used for statistical calculations are from those grids inside the solid white box, as shown in **Fig. 1a**.

As shown in **Fig. 8**, intense MCSs have the tallest average MaxHT, above 13 km. There are no differences observed in the height of MCSs in each season. However, greater variation was observed in sub-MCSs and NCs, with a storm height close to 10 km for premonsoon season. The reason for taller PFs being located over the IP during the premonsoon season is the variety and large population of Sub-MCS and NCs. The contribution of each PF type shows that NCs during post monsoon contribute the largest proportion up to 84% of all PF types. Sub-MCSs and NCs together comprise more than 95% of PF types. Using the three-dimensional structure of TRMM PR, Houze et al. (2007) found intense convective echoes occur just upstream, over the lower elevations of the Himalayas, of which sometimes extending above 17 km, indicating that exceptionally strong updraughts loft graupel

to high altitudes. The south Asian monsoon, supporting warm moisture, provides very warm and highly unstable conditions to produce orographically influenced precipitation. However, IMCSs in this study are not so intense compared to the South Asian Monsoons. Generally, over these hot spots where IMCSs are located, low-level moist air is capped by very dry air aloft to form a capping inversion situation that builds unstable layers (Houze et al., 2007).

3.3.2 Spatial Distribution of Lightning and Flash Count for Three Seasons

Based on ice scattering of convective core criteria using Min85PCT, convective systems are located on both land and sea, but spatial distribution varies among seasons (**Fig. 9**). In the premonsoon season, intense convection is sparse over the IP inland (**Fig. 9a**) and low Min85PCT is shown over the coastal areas in the eastern Gulf of Thailand and over the SCS, east of Hainan and the southern part of the SCS (**Fig. 9d**). In the monsoon season, the frequency of 85PCT is high over the northern IP (**Fig. 9b**), while intense convection occurs in the middle of the IP with relatively low intensity compared to the premonsoon and postmonsoon seasons (**Fig. 9e**). In the postmonsoon season, there is a high frequency of 85PCT located over the southern part the IP, Peninsular Malaysia, Sumatra and Borneo Islands (**Fig. 9c**). However, extremely intense convection is located over the middle and north of the IP, with relatively low 85PCT (**Fig. 9f**).

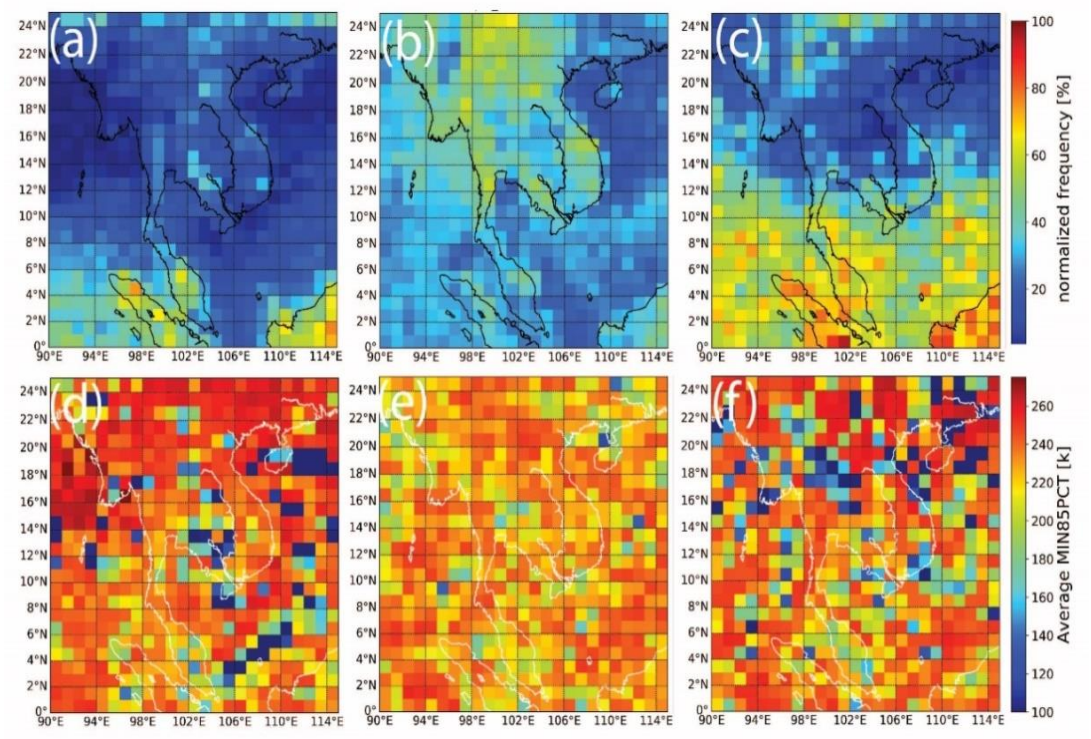

Fig. 9. PFs Locations categorized by min PCT of 85 GHz during premonsoon, monsoon, and postmonsoon (a), (b), (c) frequency of occurrences; (d), (e), (f) average. The resolution grid size is at 1° degree.

Flash count is calculated where the number is greater than zero. Generally, flash frequency over land is much greater than over open water (**Fig. 10**). The average flash count during the premonsoon season is higher than other seasons, with flash numbers exceeding 20 counts per PF over the northern region of the inland IP. Flash numbers are consistent with frequency over the IP during the premonsoon season. While the flash frequency seems high over the Malay Peninsula and north Sumatra, which is low compared to the IP. Liu et al. (2020) found that favorable environments of high flash rate thunderstorms in the tropics are characterized by higher Convective Available Potential

Energy, lower Convection Inhibition, and weaker wind shear, compared to the high flash rate thunderstorms in the subtropical regions. In the monsoon season, flash frequency increases over the IP and offshore areas in the southern region, although the flash number is relatively low compared to the premonsoon season. The finding, in this study, the higher flash rate in the premonsoon season is consistent with findings by Xu et al. (2010) regarding the flash rates before Mei-Yu onset. In the postmonsoon season, the flash frequency dramatically decreases over the IP, but it increases over the Malay Peninsula. Overall, the flash number is relatively high, but it is not consistent across the IP compared to other high frequency areas. Mao and Li (202) found that lightning activity over South China during spring, corresponding to premoonson season of this present study, has shown interannual variations and significantly correlated with El Niño‐Southern Oscillation (ENSO) by having frequent lightning in El Niño events.

There are many studies that have compared the characteristics of MCSs over both land and ocean. The enhanced convective systems over land are larger than those found over ocean regarding to structures and properties (LeMone & Zipser, 1980; Zipser & LeMone, 1980; Xu, 2013; Xu et al., 2009; Yuan & Qie, 2008). Generally, oceanic cloud systems have less intense embedded convection, but can form wide stratiform regions, while continental MCSs often have more intense embedded convection (Nesbitt et al., 2000; Houze et al., 2015; Toracinta et al., 2002). Nesbitt et al. (2000) and Toracinta et al. (2002) identified PFs using criteria of intensity and areal based on TRMM PR data by collocating them with the simultaneous passive microwave sensor measurements on frequencies of ice scattering. They found that convection over tropical landmasses is characterized by more lightning, stronger ice scattering, and more intense radar echo in the upper levels of convective clouds than in precipitating clouds over tropical oceans. Using aircraft to measure vertical draft velocities, deep convection over tropical oceans is typically found to be much lower than over land (LeMone & Zipser, 1980; Zipser & LeMone, 1980). Therefore, the high updraft velocity over land can support the generation of large supercooled water concentrations required for the graupel and hail particle formation associated with charge separation.

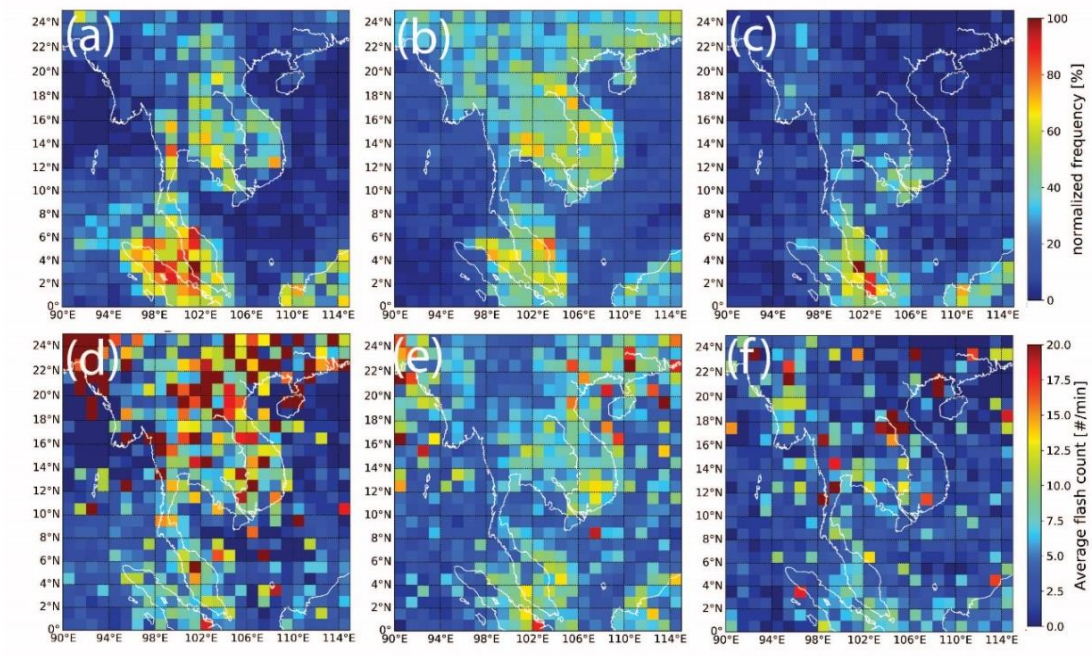

Fig. 10. Locations of PFs categorized by Flash Count during premonsoon, monsoon, and postmonsoon (a), (b), (c) frequency of occurrences; (d), (e), (f) average. The resolution grid size is at 1° degree.

4. CONCLUSIONS

Using the seasonal definitions to define onset and withdrawal dates for monsoon based on the daily TRMM 3B42 dataset, the premonsoon, monsoon and postmonsoon seasons were found for each year over the inland Indochina Peninsula (IP) and surrounding regions. Climatology of cloud properties and structure from 1998 to 2013 (16 years) over the inland and surrounding regions were investigated based on TRMM Precipitation Features (PFs) database constructed by the university of UTAH, derived from original sensors of the TRMM project. The major findings of this analysis are as follows:

Intra-seasonal and inter-seasonal variation of rainfall intensity and periodical duration are clearly found based on the applied definition to identify the seasonal period of each year. Mesoscale Convective Systems (MCSs) play a significant role for all periods. Sub-MCSs are major contributors of rainfall during the postmonsoon season, while the highest percentage of intense MCSs (IMCSs) is found during the premonsoon season. Geographically, western and northern parts of the inland IP show the most frequent occurrence of sub-MCSs and MCSs during the monsoon season, while the frequency of occurrence of MCSs and sub-MCSs during the postmonsoon season is highest over the southern part of the IP, and over sea during, respectively.

In the case of IMCSs, taller and stronger clouds (MaxHT30; MaxdBZ6) identified from PR on board TRMM are found in greater numbers over the inland IP. IMCSs in the premonsoon season are the most numerous over the inland IP, based on microwave signals and radar reflectivity sensors, with distinct spatial concentration over western and northern regions of the IP for sub-MCSs during the monsoon season. Convection intensity proxies and vertical radar reflectivity have shown intra-seasonal variation over land from cumulative density function analysis by enhancement on MCSs during the premonsoon season. The intensity of MCSs during the premonsoon season is observed through ice scattering signal (Min85PCT), MaxHT30, and MaxdBZ6. The MCSs for three periods have shown more intense properties compared to sub-MCSs. The maximum height exceeds 18 km for the premonsoon season as measured by Vertical Profile of Radar Reflectivity (VPRR).

Based on ice scattering of convective core criteria using Min85PCT, convective systems are found on both land and sea, but spatial distribution varies among seasons. Spatial variation on microphysical structure of clouds is distinctly shown by seasons based on scattering of microwave signals and lightning flash counts. Lightning is relatively more frequent over land than over surrounding ocean. The most frequent lightning over the inland IP is found during the premonsoon season, while the highest average flash count over inland IP is also found over the west, north of the IP highlands during premonsoon season. The transitional period between seasons is interesting due to the properties and structure of precipitation systems occurring over both land and oceans because the difference in microphysical clouds involved during the periods. Limitation of this study is that the fine resolution data of ground-based radar is not used to investigate in structure of extreme storm cases. Future research should attempt to elucidate this to be useful information to people to avoid the extreme weather on the transitional period. Satellite products based on TRMM legacy and ground-based radar will be used in the future analysis over the IP and surrounding seas.

5. ACKNOWLEDGEMENTS

We would like to express our gratitude the anonymous reviewers for their helpful comments and discussions. This research was supported by National Research Council of Thailand (NRCT) through the Naresuan University R2561B062 and R2562B031. We are really appreciated to “Advancing Co-design of Integrated Strategies with Adaptation to Climate Change in Thailand (ADAP-T)” supported by the Science and Technology Research Partnership for Sustainable Development (SATREPS), JST-JICA for providing research fund to support the project. Most of the figures were produced using the Python script.

REFERENCES

Balogun R.A., Adeyewa Z.D., Adefisan E.A.&Okogbue E.C. (2020) Vertical structure and frequencies of deep convection during active periods of the West and Central African monsoon season. *Theor. Appl. Climatol*., 141, 615–626

Cecil D.J., Goodman S.J., Boccippio D.J., Zipser E.J. & Nesbitt S.W. (2005) Three Years of TRMM Precipitation Features. Part I: Radar, Radiometric, and Lightning Characteristics. *Mon Wea Rev*., 133, 543–566.

Cecil D.J. & Zipser E.J. (1999) Relationships between Tropical Cyclone Intensity and Satellite-Based Indicators of Inner Core Convection: 85-GHz Ice-Scattering Signature and Lightning. *Mon Wea Rev*., 127, 103–123.

DeMott C.A. & Rutledge S.A. (1998) The Vertical Structure of TOGA COARE Convection. Part I: Radar Echo Distributions. *J Atmos Sci*., 55, 2730–2747.

Donaldson R.J. (1961) Radar Reflectivity Profiles in Thunderstorms. *J Meteorol*., 18, 292–305.

Dye J.E., Winn W.P., Jones J.J. & Breed, D.W. (1989) The Electrification of New Mexico Thunderstorms. 1. Relationship between Precipitation Development and the Onset of Electrification. *JGR*., 94, 8643–8656.

Guy N. & Rutledge S.A. (2012) Regional Comparison of West African Convective Characteristics: A TRMM-based Climatology. *QJR Meteorol Soc*., 138, 1179–1195.

Hamada A., Takayabu Y.N., Liu C. & Zipser E.J. (2015) Weak linkage between the heaviest rainfall and tallest storms. *Nat Commun*., 6, 6213.

Houze Jr. R.A. (1993) *Cloud Dynamics*. Academic Press, 573 pp.

Houze Jr. R.A. (1989) Observed Structure of Mesoscale Convective Systems and Implications for Large-scale Heating. *QJR Meteorol Soc*., 115, 425–461.

Houze Jr. R.A., Wilton D.C. & Smull B.F. (2007) Monsoon Convection in the Himalayan Region as seen by the TRMM Precipitation Radar. *QJR Meteorol Soc*., 133, 1389–1411.

Houze Jr. R.A., Zuluaga M.D. & Brodzik S.R. (2015) The Variable Nature of Convection in the Tropics and Subtropics: A Legacy of 16 years of the Tropical Rainfall Measuring Mission (TRMM) Satellite. *Rev Geophys*, 53, 994–1021.

Huffman G.J. & Coauthors. (2007) The TRMM Multisatellite Precipitation Analysis (TMPA): Quasi-global, Multiyear, Combined-Sensor Precipitation Estimates at Fine Scales. *J. Hydrometeorol*., 8, 38–55.

Jorgensen D.P. (1984) Mesoscale and Convective-scale Characteristics of Mature Hurricanes. Part I: General Observations by Research Aircraft. *J Atmos Sci*., 41, 1268–1285.

Kodama C., Yamada Y., Noda A.T., Kikuchi K., Kajikawa Y., Nasuno T., Tomita T., Yamaura T., Takahashi H.G., Hara M., Kawatani Y., Satoh M. & Sugi M. (2015) A 20-year climatology of a NICAM AMIP-type simulation. *J Meteorol Soc Japan*., 93:393–424.

Kodama Y.-M., Ohta A., Katsumata M., Mori S., Satoh S. & Ueda H. (2005) Seasonal Transition of Predominant Precipitation Type and Lightning Activity over Tropical Monsoon Areas derived from TRMM Observations. *Geophys Res Lett*., 32, L14710.

Kummerow C., Barnes W., Kozu T., Shiue J. & Simpson J. (1998) The Tropical Rainfall Measuring Mission (TRMM) Sensor Package. *J Atmos Ocean Technol*., 15, 809–817.

LeMone M.A. & Zipser E.J. (1980) Cumulonimbus Vertical Velocity Events in GATE. Part I: Diameter, Intensity, and Mass Flux. *J Atmos Sci*., 37, 2444–2457.

Li N., Wang Z., Chen X. & Austin G. (2019) Studies of General Precipitation Features with TRMM PR Data: An Extensive Overview. *Remote Sensing*., 11, 80.

Liu C. (2013) University of Utah TRMM Precipitation and Cloud Feature Database Description Version 2.0, Department of Atmospheric Sciences, University of Utah, 33pp.

Liu C. & Zipser E.J. (2005) Global Distribution of Convection Penetrating the Tropical Tropopause. *JGR*, 110.

Liu C., Zipser E.J., Cecil D.J., Nesbitt S.W. & Sherwood S.A. (2008) Cloud and Precipitation Feature Database from Nine Years of TRMM Observations. *J Appl Meteorol Climatol*., 47, 2712–2728.

Liu C., Zipser E.J. & Nesbitt S.W. (2007) Global Distribution of Tropical Deep Convection: Different Perspectives from TRMM Infrared and Radar Data. *J. Clim*., 20, 489–503.

Liu N., Liu C., Chen B. & Zipser E. (2020) What Are the Favorable Large-Scale Environments for the Highest-Flash-RateThunderstorms on Earth?.*J Atmos Sci*., 77, 1583–1612.

Matsumoto J. (1997) Seasonal Transition of Summer Rainy Season over Indochina and Adjacent Monsoon Region. *Adv. Atmos. Sci*., 14, 231–245.

Mao J. & Li M. (2020) Interannual variations in spring lightning activity and convective rainfall over South China during the TRMM era. Theor. Appl. Climatol., 142, 483‑495.

McGaughey G.R., Zipser E.J., Spencer R.W. & Hood R.E. (1996) High-Resolution Passive Microwave Observations of Convective Systems over the Tropical Pacific Ocean. *J Appl Meteorol*., 35, 1921–1947.

Medina S., Houze Jr. R.A., Kumar A. & Niyogi D. (2010) Summer Monsoon Convection in the Himalayan region: Terrain and Land Cover Effects. *QJR Meteorol Soc*., 136, 593–616.

Mohr K.I. & Zipser E.J. (1996) Mesoscale Convective Systems Defined by Their 85-GHz Ice Scattering Signature: Size and Intensity Comparison over Tropical Oceans and Continents. *Mon Wea Rev*., 124, 2417–2437.

Nesbitt S.W. & Zipser E.J. (2003) The Diurnal Cycle of Rainfall and Convective Intensity according to Three Years of TRMM Measurements. *J Clim*., 16, 1456-1475.

Nesbitt S.W., Zipser E.J. & Cecil D.J. (2000) A Census of Precipitation Features in the Tropics Using TRMM: Radar, Ice Scattering, and Lightning Observations. *J Clim*., 13, 4087–4106.

Nesbitt S.W., Zipser E.J. & Kummerow C.D. (2004) An Examination of Version-5 Rainfall Estimates from the TRMM Microwave Imager, Precipitation Radar, and Rain Gauges on Global, Regional, and Storm Scales. *J Appl Meteorol*., 43, 1016–1036.

Petersen W.A., Cifelli R.C., Rutledge S.A., Ferrier B.S. & Smull B.F. (1999) Shipborne Dual-Doppler Operations during TOGA COARE: Integrated Observations of Storm Kinematics and Electrification. *Bull Am Meteorol Soc*., 80, 81–96.

Petersen W.A., Nesbitt S.W., Blakeslee R.J., Cifelli R., Hein P. & Rutledge S.A. (2002) TRMM Observations of Intraseasonal Variability in Convective Regimes over the Amazon. *J. Clim*., 15, 1278–1294.

Petersen W.A & Rutledge S.A. (2001) Regional Variability in Tropical Convection: Observations from TRMM. *J Clim*., 14, 3566–3586.

Petersen W.A., Rutledge S.A. & Orville R.E. (1996) Cloud-to-Ground Lightning Observations from TOGA COARE: Selected Results and Lightning Location Algorithms. *Mon Wea Rev*., 124, 602–620.

Qie X., Toumi R. & Yuan T. (2003) Lightning Activities on the Tibetan Plateau as Observed by the Lightning Imaging Sensor. *JGR*., 108, 4551.

Rapp A.D., Peterson A.G., Frauenfeld O.W., Quiring S.M. & Roark E.B. (2014) Climatology of Storm Characteristics in Costa Rica using the TRMM Precipitation Radar. *J. Hydrometeorol*., 15, 2615–2633.

Romatschke U. & Houze Jr. R.A. (2010) Extreme summer convection in South America. *J Clim*., 23, 3761–3791.

Satoh M., Noda A.T., Seiki T., Chen Y.-W., Kodama C., YamadaY., Kuba N. & Sato Y. (2018) Toward reduction of the uncertainties in climate sensitivity due to cloud processes using a global non-hydrostatic atmospheric model. *PEPS*., 5, 67.

Saunders, C.P.R. & Peck, S.L. (1998) Laboratory Studies of the Influence of the Rime Accretion Rate on Charge Transfer during Crystal/Graupel Collisions. *JGR*., 103.

Spencer R.W., Goodman H.G. & Hood R.E. (1989) Precipitation Retrieval over Land and Ocean with the SSM/I: Identification and Characteristics of the Scattering Signal. *J Atmos Ocean Technol*., 6, 254–273.

Szoke E.J. & Zipser E.J. (1986) A Radar Study of Convective Cells in Mesoscale Systems in GATE. Part II: Life Cycles of Convective Cells. *J. Atmos. Sci*., 43, 199–218.

Takahashi H. & Yasunari T. (2006) A Climatological Monsoon Break in Rainfall over Indochina−A Singularity in the Seasonal March of the Asian Summer Monsoon. *J. Climate.*, 19, 1545–1556.

Toracinta E.R., Cecil D.J., Zipser E.J. & Nesbitt S.W. (2002) Radar, Passive Microwave, and Lightning Characteristics of Precipitating Systems in the Tropics. *Mon Wea Rev*., 130(4), 802–824.

Vivekanandan J., Turk J. & Bringi V.N. (1991) Ice Water Path Estimation and Characterization Using Passive Microwave Radiometry. *J Appl Meteorol*.. 30, 1407–1421.

Wang B. & Ho L. (2002) Rainy Season of the Asian–Pacific Summer Monsoon. *J.Climate*., 15, 386–397.

Williams E.R. (1989) The Tripole Nature of Thunderstorms. *JGR*., 94, 13 151–13 167.

Williams E.R., Rutledge S.A., Geotis S.G., Renno N., Rasmussen E. & Rickenbach T. (1992) A Radar and Electrical Study of Tropical "Hot Towers". *J Atmos Sci*., 49, 1386–1395.

Xu W. (2013) Precipitation and Convective Characteristics of Summer Deep Convection over East Asia Observed by TRMM. *Mon Wea Rev*., 141, 1577–1592.

Xu W., Zipser E.J. & Liu C. (2009) Rainfall Characteristics and Convective Properties of Mei-Yu Precipitation Systems over South China, Taiwan, and the South China Sea. Part I: TRMM Observations. *Mon Wea Rev*., 137, 4261–4275.

Xu W., Zipser E.J., Liu C. & Jiang H. (2010) On the Relationships between Lightning Frequency and Thundercloud Parameters of Regional Precipitation Systems. *JGR*., 115, D12203.

Yokoyama C. & Takayabu Y.N. (2008) A Statistical Study on Rain Characteristics of Tropical Cyclones Using TRMM Satellite Data. *Mon Wea Rev*., 136, 3848–3862.

Yuan T. & Qie X. (2008) Study on Lightning Activity and Precipitation Characteristics before and after the Onset of the South China Sea Summer Monsoon. *JGR*., 113, D14101.

Zipser E.J., Cecil D.J., Liu C., Nesbitt S.W. & Yorty D.P. (2006) Where are the most intense thunderstorms on earth? *Bull. Am. Meteorol. Soc*., 87, 1057–1071.

Zipser E.J. & LeMone M.A. (1980) Cumulonimbus Vertical Velocity Events in GATE. Part II: Synthesis and Model Core Structure. *J Atmos Sci*., 37, 2458–2469.

Zipser E.J. & Lutz K.R. (1994) The Vertical Profile of Radar Reflectivity of Convective Cells: A Strong Indicator of Storm Intensity and Lightning Probability? *Mon Wea Rev*., 122, 1751–1759.